



Structure of the *Bacillus subtilis* hibernating 100S ribosome reveals the basis for 70S dimerization

Bertrand Beckert^{1,†}, Maha Abdelshahid^{1,†}, Heinrich Schäfer², Wieland Steinchen³, Stefan Arenz¹, Otto Berninghausen¹, Roland Beckmann¹, Gert Bange^{3,*} , Kürşad Turgay^{2,**}  & Daniel N Wilson^{1,4,***} 

Abstract

Under stress conditions, such as nutrient deprivation, bacteria enter into a hibernation stage, which is characterized by the appearance of 100S ribosomal particles. In *Escherichia coli*, dimerization of 70S ribosomes into 100S requires the action of the ribosome modulation factor (RMF) and the hibernation-promoting factor (HPF). Most other bacteria lack RMF and instead contain a long form HPF (LHPF), which is necessary and sufficient for 100S formation. While some structural information exists as to how RMF and HPF mediate formation of *E. coli* 100S (*Ec*100S), structural insight into 100S formation by LHPF has so far been lacking. Here we present a cryo-EM structure of the *Bacillus subtilis* hibernating 100S (*Bs*100S), revealing that the C-terminal domain (CTD) of the LHPF occupies a site on the 30S platform distinct from RMF. Moreover, unlike RMF, the *Bs*LHPF-CTD is directly involved in forming the dimer interface, thereby illustrating the divergent mechanisms by which 100S formation is mediated in the majority of bacteria that contain LHPF, compared to some γ -proteobacteria, such as *E. coli*.

Keywords cryo-EM; hibernation; HPF; RMF; translation

Subject Categories Microbiology, Virology & Host Pathogen Interaction; Protein Biosynthesis & Quality Control; Structural Biology

DOI 10.15252/embj.201696189 | Received 28 November 2016 | Revised 26 March 2017 | Accepted 29 March 2017 | Published online 3 May 2017

The EMBO Journal (2017) 36: 2061–2072

See also: I Khusainov *et al* (July 2017) and RL Gonzalez Jr (July 2017)

Introduction

The translational activity of the bacterial cell is able to respond rapidly to a variety of environmental cues. This is exemplified by the decrease in translational activity observed in bacteria entering into stationary growth phase due to stress conditions, such as nutrient

deprivation. Under such circumstances, the decrease in translational activity is correlated with the appearance of 100S particles, which arise due to the dimerization of 70S ribosomes (Wada *et al*, 1990), reviewed by Yoshida and Wada (2014). In *E. coli*, 100S formation requires the presence of the ribosome modulation factor (RMF) and the hibernation-promoting factor (HPF, previously referred to as YhbH; Yamagishi *et al*, 1993; Wada *et al*, 1995; Maki *et al*, 2000; Ueta *et al*, 2005, 2008). Stationary phase *E. coli* cells also express a homolog of HPF (Fig 1A), termed YfiA (also referred to as pY or RaiA), which binds and inactivates 70S ribosomes (Agafonov & Spirin, 2004; Vila-Sanjurjo *et al*, 2004), and is antagonistic to RMF and HPF action by preventing 100S formation (Maki *et al*, 2000; Ueta *et al*, 2005). The hibernation state (Yoshida *et al*, 2002) appears to be important for bacterial survival since inactivation of the *rmf* gene leads to loss of viability in stationary phase cells (Yamagishi *et al*, 1993; Wada *et al*, 2000; Shcherbakova *et al*, 2015) as well as increased sensitivity to osmotic (Garay-Arroyo *et al*, 2000), heat (Niven, 2004), and acid stress (El-Sharoud & Niven, 2007).

Phylogenetic analyses have revealed that the presence of RMF and HPF is restricted to a subset of γ -proteobacteria, including *E. coli*, whereas the majority of other bacteria lack both RMF and YfiA, and instead contain a long form of HPF (LHPF; Fig 1A; Ueta *et al*, 2008, 2013; Yoshida & Wada, 2014). LHPFs comprise an N-terminal domain (NTD) homologous to the short form HPF (SHPF) and a unique C-terminal domain (CTD; Fig 1A), which was proposed to have weak homology with RMF (Ueta *et al*, 2010). LHPFs have been shown to be necessary and sufficient for 100S formation in a variety of different bacteria, including *Staphylococcus aureus* (Ueta *et al*, 2010, 2013; Basu & Yap, 2016), *Lactobacillus paracasei*, *Thermus thermophilus* (Ueta *et al*, 2010, 2013), *Lactococcus lactis* (Puri *et al*, 2014), and *B. subtilis* (Tagami *et al*, 2012; Akanuma *et al*, 2016). Unlike *E. coli* SHPF-100S (*Ec*100S), low levels of LHPF-containing 100S are also observed in exponentially growing cells (Ueta *et al*, 2010, 2013; Akanuma *et al*, 2016). Proteomics studies indicate that expression levels of *Bs*LHPF increase under conditions of nutrient deprivation, but also in response to antibiotics, heat, salt, and ethanol stress (Drzewiecki *et al*, 1998;

1 Gene Center, Department for Biochemistry and Center for integrated Protein Science Munich (CiPSM), University of Munich, Munich, Germany

2 Naturwissenschaftliche Fakultät, Institut für Mikrobiologie, Leibniz Universität Hannover, Hannover, Germany

3 LOEWE Center for Synthetic Microbiology and Faculty of Chemistry, Philipps University Marburg, Marburg, Germany

4 Institute for Biochemistry and Molecular Biology, University of Hamburg, Hamburg, Germany

*Corresponding author. Tel: +49 64 2128 23361; E-mail: gert.bange@synmikro.uni-marburg.de

**Corresponding author. Tel: +49 511 7625241; E-mail: turgay@ifmb.uni-hannover.de

***Corresponding author. Tel: +49 40 4283 82841; E-mail: Daniel.Wilson@chemie.uni-hamburg.de

†These authors contributed equally to this work

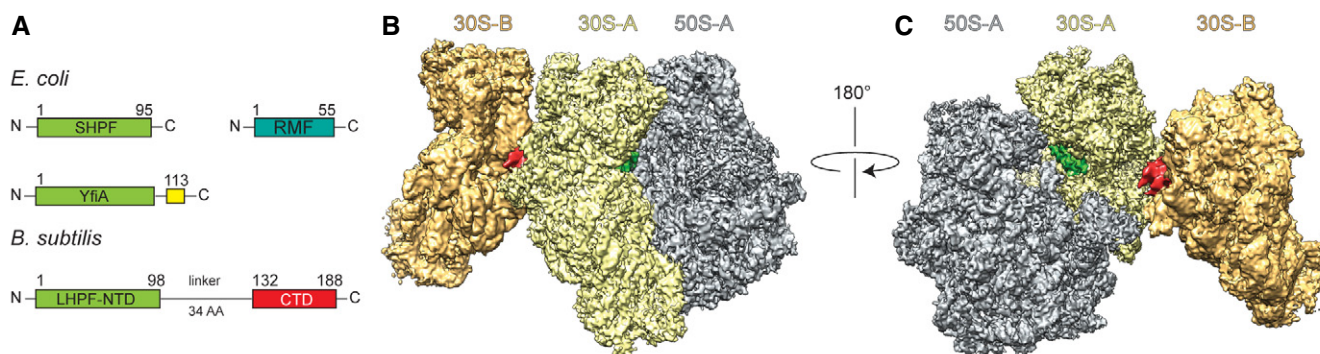


Figure 1. Cryo-EM reconstruction of the *Bs*70S-30S subcomplex.

- A Schematic representation of the domain structure of *Escherichia coli* short form HPF (SHPF), RMF, and YfiA (C-terminal extension in yellow) compared to *Bacillus subtilis* long form HPF (LHPF) harboring an N-terminal (NTD, green) and C-terminal domains (CTD, red).
- B, C Two views of the cryo-EM map of the *Bs*70S-30S subcomplex, with separated densities for the 30S-A (yellow), 50S-A (gray), 30S-B (orange), and additional densities in green and red.

Reiss *et al.*, 2012; Tagami *et al.*, 2012). In *Listeria monocytogenes*, LHPF is necessary for tolerance of bacteria to aminoglycoside antibiotics during stationary phase (McKay & Portnoy, 2015) and for optimal fitness and pathogenesis (Kline *et al.*, 2015).

Cryo-EM and cryo-electron tomography (cryo-ET) structures of the *Ec*100S have revealed that the 70S monomers interact with each other via the back of the 30S subunits (Kato *et al.*, 2010; Ortiz *et al.*, 2010), consistent with earlier negative stain images (Wada, 1998; Yoshida *et al.*, 2002). Unfortunately, the low resolution (18–38 Å) of these structures was insufficient to resolve the binding positions of the RMF and SHPF proteins within the *Ec*100S (Kato *et al.*, 2010; Ortiz *et al.*, 2010). However, structures of *E. coli* SHPF and RMF were subsequently determined on the *T. thermophilus* 70S ribosome by X-ray crystallography (Polikanov *et al.*, 2012), providing insight into how SHPF and RMF dimerize 70S ribosomes and inactivate translation in γ -proteobacteria. To date, there is, however, little structural information available as to how LHPFs interact with 70S ribosomes to mediate 100S formation in the majority of bacteria other than *E. coli* and its close relatives.

Here we present a cryo-EM structure of the *B. subtilis* 100S particle (*Bs*100S) revealing the binding site for the *Bs*HSPF (also referred to as YvyD). The *Bs*HSPF-NTD binds in a position overlapping the mRNA, A- and P-tRNAs, analogous to YfiA, SHPF, and the NTD of the LHPF from spinach chloroplasts (Vila-Sanjurjo *et al.*, 2004; Sharma *et al.*, 2007, 2010; Polikanov *et al.*, 2012; Graf *et al.*, 2016; Bieri *et al.*, 2017), indicating how LHPFs inhibit translation (Ueta *et al.*, 2013; Basu & Yap, 2016). Unexpectedly, we observe that the *Bs*HSPF-CTD forms a homodimer with the CTD of the *Bs*HSPF from the second 70S ribosome, thus providing a structural basis for LHPF-mediated 100S formation. Our findings reveal that 100S formation mediated by RMF and HPF in γ -proteobacteria, such as *E. coli*, is mechanistically unrelated to 100S formation mediated by LHPF in the majority of other bacteria.

Results

Cryo-EM structure of *Bs*100S

*Bs*100S ribosomal particles were isolated from lysates of late exponential phase cells using sucrose density gradient

centrifugation (Fig EV1A, see Materials and Methods). Negative stain electron microscopy images of the isolated *Bs*100S revealed the characteristic dimer arrangement of 70S monomers interacting via their 30S subunits (Fig EV1B), as observed previously for *B. subtilis* (Tagami *et al.*, 2012), *Lactococcus lactis* (Puri *et al.*, 2014), but distinct from *Ec*100S (Wada, 1998; Yoshida *et al.*, 2002; Kato *et al.*, 2010). The presence of the *Bs*HSPF (YvyD) in the *Bs*100S was further confirmed using mass spectrometry. The LHPF-containing 100S particles were then subjected to single particle cryo-EM analysis (see Materials and Methods). Processing of the *Bs*100S was performed by aligning the 70S ribosomes within each 100S to a vacant 70S reference. The box size was maintained large enough so that the majority of the small 30S subunit of the second 70S ribosome in the dimer would also be represented during the reconstruction. The initial reconstructions revealed significant flexibility in the 100S, which was indicated by a stable aligned ribosome (70S-A) with a blurred density for the second 70S ribosome (70S-B). By implementing *in silico* sorting procedures, we were able to obtain a subpopulation of 100S particles with better-defined density for the 70S-B ribosome (Fig EV2). Subsequent refinement yielded a cryo-EM reconstruction of the *Bs*70S-30S subcomplex (Fig 1B and C) with an average resolution of 3.8 Å (Fig EV3A–D and Table EV1). Local resolution calculations indicate that the resolution for the 70S-A monomer ranges in the core between 3.5 and 5.0 Å, whereas, as expected, the resolution for 70S-B is worse, ranging between 5.0 and 10 Å (Fig EV3B and C). The cryo-EM map was fitted with the molecular model of the *B. subtilis* 70S ribosome (Sohmen *et al.*, 2015), revealing that the 70S-A monomer adopts a classic non-rotated state, as observed previously (Sohmen *et al.*, 2015). Moreover, the swivel of head observed when *E. coli* SHPF and RMF bind to *T. thermophilus* 70S ribosomes (Polikanov *et al.*, 2012) is not observed in the *Bs*100S, indicating that dimerization of *B. subtilis* 70S ribosomes, unlike *E. coli*, does not require head movement. After fitting of the 70S models, two unassigned densities remained, one located within the intersubunit space of the 70S-A ribosome and a second located on the back of the 30S platform at the interface of the 70S-A and 70S-B ribosomes (Fig 1B and C).

Binding site of the BsHPPF-NTD on the small 30S subunit

The additional map density within the intersubunit space located between the head and body of the 30S subunit was assigned to the N-terminal domain of BsHPPF (BsHPPF-NTD; Fig 2A). This was based on the high sequence similarity of the BsHPPF-NTD with *E. coli* YfiA and HPF (Fig EV1C), both of which were shown to bind to this region of the ribosome (Vila-Sanjurjo *et al*, 2004; Polikanov *et al*, 2012). The local resolution of the BsHPPF-NTD ranged between 3.5 and 5.0 Å (Fig EV3F–G), enabling an unambiguous fit of the homology model to the density (Fig 2B). Aligning the *E. coli* SHPF-70S structure (Polikanov *et al*, 2012) to the 70S-A ribosome in the Bs100S based on the 16S rRNA revealed the expected similarity in their binding positions (Fig 2C). As noted previously for *E. coli* YfiA and HPF (Vila-Sanjurjo *et al*, 2004; Polikanov *et al*, 2012) and for the NTD of the LHPF from Spinach chloroplast (Sharma *et al*, 2007, 2010; Graf *et al*, 2016; Bieri *et al*, 2017), the binding position of BsHPPF-NTD overlaps with the mRNA and anticodon-stem loop regions of tRNAs bound in the ribosomal A- and P-sites (Fig 2D), thus explaining the observed inhibitory effect by LHPFs when added to *in vitro* translation assays (Ueta *et al*, 2013; Basu & Yap, 2016). The BsHPPF-NTD is connected by a 34 aa linker to the CTD (Fig 1A). Map density for the linker region was not observed in the cryo-EM map of the Bs100S, indicating that it is highly flexible. An exception is the 5–6 aa stretch of the linker region that directly follows the terminal α -helix of the BsHPPF-NTD (Fig 2B). Map density for this N-terminal part of the linker passes, analogous to mRNA, through the opening created by the β -hairpin of ribosomal protein S7 and helix h23 of the 16S rRNA, and extends in the general direction of the platform cavity at the back of the 30S subunit (Fig EV4).

BsHPPF-CTD is present as a dimer on the small 30S subunit

Given the general direction of the linker, we assigned the additional density located on the back of the 30S platform to the BsHPPF-CTD (Fig 3A and B). It was possible to generate a homology model for the BsHPPF-CTD based on the deposited crystal structure of the LHPF-CTD from a closely related Firmicute, *Clostridium acetobutylicum* (PDB ID 3KA5; Fig EV1D). Curiously, the *C. acetobutylicum* LHPF-CTD is present as a dimer in the crystal, and it was possible to make an unambiguous rigid body fit of the homology model of the BsHPPF-CTD dimer into the unassigned map density of the cryo-EM map (Fig 3C). We note that while the structurally conserved *L. monocytogenes* HPF-CTD (PDB ID 3K2T) appears as a monomer in the asymmetric unit, the homodimer forms across the crystallographic twofold symmetry. This suggests that the LHPF-CTDs are not only dimeric on the ribosome, but are likely to be dimeric in solution. To investigate this further, we performed size-exclusion chromatography (SEC) on the recombinantly expressed and purified wild-type BsHPPF and BsHPPF variants (see Materials and Methods). Analysis of the full-length BsHPPF and the BsHPPF-CTD revealed that they have apparent molecular masses of 56 and 14 kDa, respectively, rather than the expected 23 kDa and 8 kDa (Fig 3D–G), indeed suggesting that both proteins are dimeric in solution as well as on the ribosome. The apparent migration behavior of BsHPPF on SEC reflects the elongated shape of the dimer as also seen in our cryo-EM structure of the Bs100S. Based on the structures of the dimeric *C. acetobutylicum* and *L. monocytogenes*

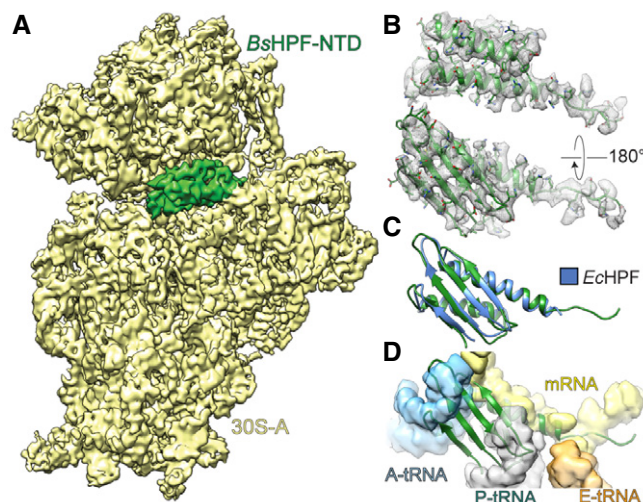


Figure 2. Interaction of the BsHPPF-NTD with the ribosome.

- A Interface view of cryo-EM map of the 30S-A (yellow) from the Bs70S-30S subcomplex with separated BsHPPF-NTD density (green).
 B Map density (gray mesh) with model of BsHPPF-NTD (green).
 C, D Comparison of BsHPPF-NTD (green) with (C) *Escherichia coli* SHPF (EcHPF, blue; Polikanov *et al*, 2012), and (D) mRNA (yellow surface), A- (cyan), P- (gray), and E-tRNAs (orange; Jenner *et al*, 2011).

LHPF-CTD, we rationalized that the highly conserved Phe160 in the BsHPPF-CTD is critical for dimerization (Fig 3H). Phe160 is present within the very hydrophobic dimer interface where it forms stacking interactions with Phe160 of the second monomer (Fig 3H). We predicted that a mutation of Phe160 to Glu (F160E) would disrupt the dimer interface via introduction of a negative charge into the hydrophobic environment. To test this, we also subjected the full-length BsHPPF-F160E protein to SEC (Fig 3D and E), revealing that the protein eluted with an apparent molecular mass of 40 kDa, smaller than the 56 kDa observed for the wild-type BsHPPF (Fig 3G). Although 40 kDa is larger than the expected size of 22.8 kDa, we believe this is due to retardation of the NTD and subsequent linker. Indeed, a BsHPPF variant lacking the CTD (BsHPPF-NTD) eluted with an apparent molecular mass of 28 kDa (rather than the expected 13.1 kDa; Fig 3G). This observation is in good agreement with structural information on the NTDs of other hibernation factors showing a non-globular shape (Polikanov *et al*, 2012). Our conclusions based on SEC were also confirmed using static light scattering (SLS), revealing the full-length BsHPPF had an absolute molecular mass of 42.8 ± 0.9 kDa, corresponding with a dimer (46 kDa), whereas the mass of the BsHPPF-F160E variant (28 ± 2.1 kDa) was more consistent with a monomer (22.8 kDa; Fig 3G). Taken together, our biochemical data clearly show that BsHPPF forms a homodimer in solution that is mediated via its CTD.

Dimerization of 70S ribosomes via the BsHPPF-CTD

While the limited resolution of the BsHPPF-CTD (Fig EV3H and I) does not allow a detailed analysis of the contacts with the ribosomal components to be made, the fitted model nevertheless enables a general description of the interaction mode (Fig 4A). The BsHPPF-CTD appears to interact exclusively with ribosomal proteins S2 and

S18 and does not establish contact with the 16S rRNA. Importantly, each *Bs*HPF-CTD monomer contacts S2 from the 70S to which the corresponding *Bs*HPF-NTD is bound, whereas the interaction with the N-terminal extension of S18 is from the second 70S ribosome (Fig 4A). The 100S dimer is also stabilized by direct interactions between the 70S-A and 70S-B monomers (Fig 4A and B). In addition to the contacts established between the N-terminal helix of S2 and the N-terminal extension of S18, the N-terminal β -hairpin and proximal region of the α 2-helix of S2 establish a large interaction surface with the stem-loop of helix h26 of the 16S rRNA of the second 70S (Fig 4B). Thus, the dimerization of the HPF-CTDs stabilizes and facilitates direct interaction between the 70S-A and 70S-B monomers in the *Bs*100S. Our findings highlight the importance of the *Bs*HPF-CTD for 70S dimerization, and therefore 100S formation, which is in complete agreement with biochemical studies demonstrating that truncation of the CTD from LHPF leads to loss of 100S formation (Puri *et al*, 2014; Basu & Yap, 2016). Moreover, it was reported that the CTD of the LHPF from *Lactococcus lactis* can dimerize *E. coli* 70S ribosomes, but only when acting in concert with the SHPF from *E. coli* (Puri *et al*, 2014). This observation supports to some extent the previous assertion that the HPF-CTD functions analogously to RMF; an assertion that was partly based on proposed sequence homology between HPF-CTD and RMF (Ueta *et al*, 2010). However, comparison of the structures of *Bs*HPF-CTD with that of RMF on the ribosome (Polikanov *et al*, 2012) reveals that there is no structural similarity in terms of the protein fold and, despite both binding at the platform region at the back of the 30S subunit, there is no overlap in their binding sites on the ribosome (Fig 4C). The binding position of RMF was suggested to inhibit translation by sterically preventing formation of the Shine-Dalgarno-helix (SD-helix) between the 5' end of the mRNA and the 3' end of the 16S rRNA (Polikanov *et al*, 2012). In contrast, the HPF-CTD does not overlap with the SD-helix (Fig 4D), although we cannot exclude the possibility that the flexible linker of *Bs*HPF traverses the RMF binding site since it was not visualized in the cryo-EM map.

Importance of the linker-CTD for 100S formation

To assess the importance of the linker and CTD of *Bs*HPF for 100S formation *in vivo*, we generated a *B. subtilis* 168 strain where the *yvyD* gene was inactivated (Δ *Bs*HPF), as confirmed by Western blotting using antibodies specific to *Bs*HPF (Fig 5A). We then re-introduced the wild-type *yvyD* gene, as well as *yvyD* variants, into the *amyE* locus and monitored the IPTG-induced expression of the *Bs*HPFs (Fig 5A). To investigate the importance of the linker between the NTD and CTD of *Bs*HPF, we generated Δ *Bs*HPF strains expressing *Bs*HPF deletion variants lacking 10 aa (*Bs*HPF-L Δ 10AA, lacking residues 110–119) or 20 aa (*Bs*HPF-L Δ 20AA, lacking residues 105–124) from the central region of the linker (Fig 5A). In addition, we generated a *Bs*HPF variant bearing the F160E mutation in the CTD (*Bs*HPF-F160E), which interferes with homodimerization (Fig 3G). Western blotting of cell extracts from stationary phase bacteria indicated that all *Bs*HPF variants inserted into the *amyE* locus were expressed in the presence of IPTG at similar levels to wild-type *Bs*HPF observed in the parental *Bs*168 strain (Fig 5A). Pelleting experiments indicated that full-length *Bs*HPF co-migrated with the ribosome fraction as expected, as did the *Bs*HPF-L Δ 10AA variant (Fig 5B). In contrast, the *Bs*HPF-L Δ 20AA

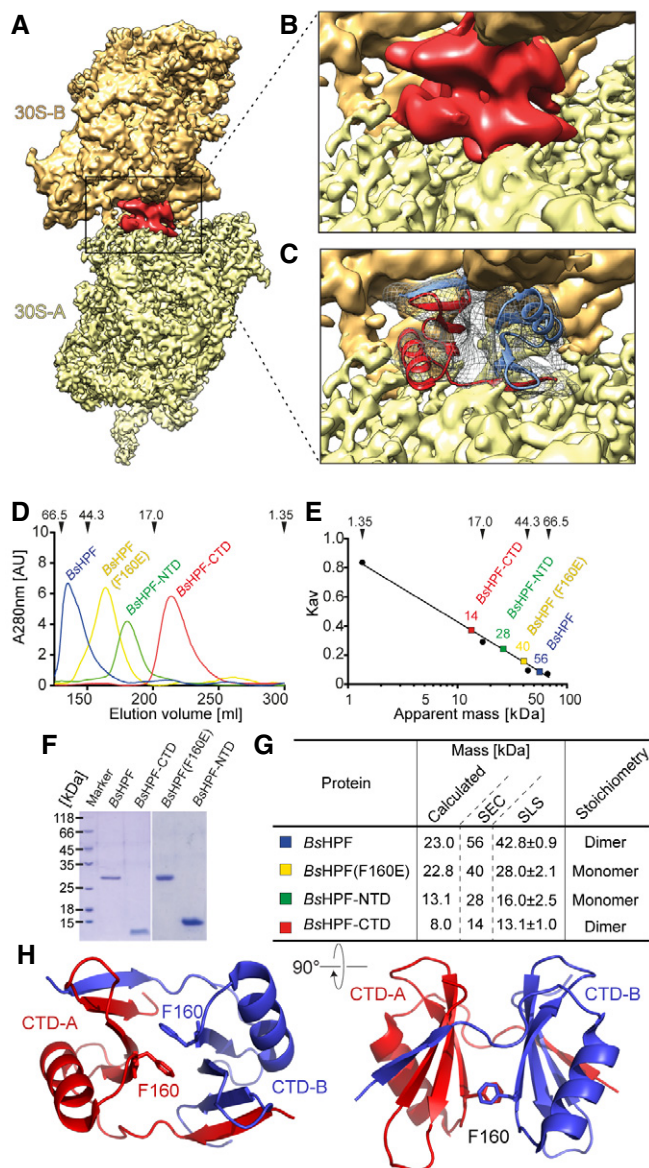


Figure 3. Binding site of dimeric LHPF-CTD on the *Bs*70S-30S subcomplex.

- A Cryo-EM map of the 30S-A (yellow) from the *Bs*70S-30S subcomplex with separated LHPF-CTD density (red).
- B, C Density (gray mesh) with fitted model of dimeric LHPF-CTD with monomers from 70S-A and 70S-B colored red and blue, respectively.
- D Gel-filtration profiles of full-length *Bs*HPF (blue), *Bs*HPF-F160E (yellow), *Bs*HPF-NTD (green), and *Bs*HPF-CTD (red). Arrows indicate the molecular mass in kDa of the size standard.
- E Standard curve with estimated molecular masses for full-length *Bs*HPF (blue), *Bs*HPF-F160E (yellow), *Bs*HPF-NTD (green), and *Bs*HPF-CTD (red). Arrows indicate the molecular mass in kDa of the size standard.
- F Coomassie-stained SDS-PAGE of the peak fractions containing *Bs*HPF or its variants.
- G Table summarizing the actual and apparent molecular mass of proteins in (D-F). Size-exclusion chromatography (SEC) and static light scattering (SLS) determined the apparent and absolute MWs, respectively. "Stoichiometry" indicates whether *Bs*HPF and its variants exist as mono- or homodimer.
- H Homology model of the *Bs*HPF-CTD homodimer illustrating the position of Phe160 (F160) at the dimer interface.

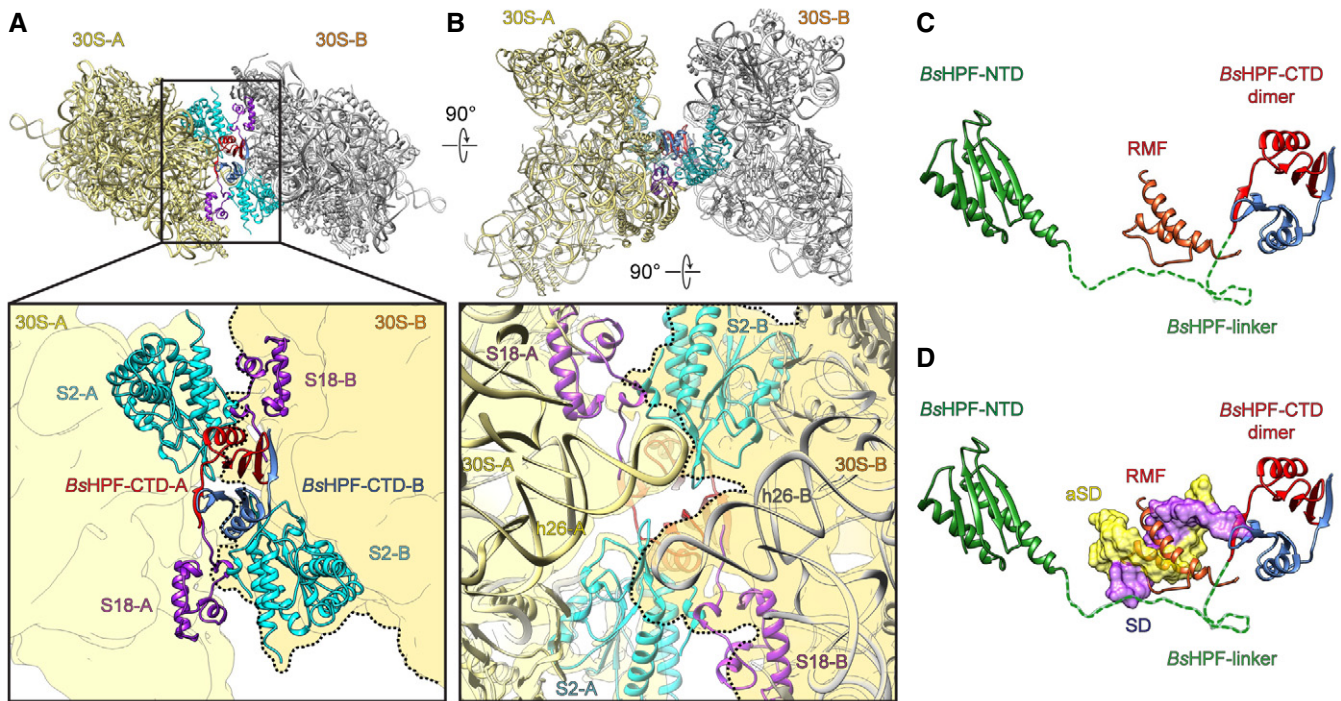


Figure 4. Dimerization interface of the *Bs*70S-30S subcomplex.

A, B Distinct views of the dimer interface between 30S-A (yellow) with BsHHPF-CTD-A (red) and 30S-B (gray, darker yellow with dashed line in zoomed panel) with BsHHPF-CTD-B (blue). Ribosomal proteins S2 (cyan), S18 (purple), and 16S rRNA are shown only, and the surface outline of the 30S subunit is included schematically for reference.

C, D Binding site of BsHHPF-NTD (green) and dimeric BsHHPF-CTD (red, blue) relative to (C) RMF (orange; Polikanov *et al.*, 2012) and (D) SD–anti-SD helix (yellow-purple surface; Sohmen *et al.*, 2015). The dashed line indicates the linker and is shown only to illustrate that the 34 amino acids are more than sufficient to connect the NTD and CTD; however, no density for the linker was observed, suggesting it does not adopt a defined conformation on the ribosome.

and BsHHPF-F160E variants had significantly reduced association with the ribosomal pellets (Fig 5B), suggesting that the deletion of 20 aa within the linker or preventing homodimerization via the CTD disrupts the interaction of BsHHPF with the ribosome. This is consistent with previous studies using *S. aureus* LHPF where C-terminal truncations of 42 aa (Δ CTD) and 90 aa (Δ linker–CTD) led to progressive loss in ribosome binding (Basu & Yap, 2016).

We next employed sucrose density gradient centrifugation to monitor the formation of 100S ribosomes using the different *Bs*168 strains (Fig 5C–G). As controls, the wild-type *Bs*168 strain was harvested during exponential phase, where a large 70S peak and lots of polysomes were observed, but little or no 100S were evident (Fig 5C). In contrast, a short heat treatment of the wild-type cells led to a complete loss of polysomes and the appearance of a prominent 100S peak (Fig 5C), as observed previously for *B. subtilis* (Akanuma *et al.*, 2016). Formation of 100S was never observed in the Δ BsHHPF strain (Fig 5C) regardless of the stress conditions tested, in agreement with the strict dependence on BsHHPF for 70S dimerization (Akanuma *et al.*, 2016). However, when the *yvyD* gene was reintroduced into the *amyE* locus of the Δ BsHHPF strain, 100S formation (and loss of polysomes) was observed, but only when BsHHPF expression was induced by the presence of IPTG (Fig 5D). No significant increase in the 100S peak, nor reduction in polysomes, was observed when

expression of the BsHHPF-L Δ 20AA variant was induced (Fig 5E), consistent with the lack of ribosome binding (Fig 5B). Surprisingly, similar results were obtained for BsHHPF-L Δ 10AA (Fig 5F), suggesting that although the BsHHPF-L Δ 10AA can still bind to the ribosome (Fig 5B), it is impaired in 100S formation. BsHHPF variants where the 10 aa or 20 aa were substituted (rather than deleted) by glycine-serine (GS) repeats, creating BsHHPF-(GS)₅ or BsHHPF-(GS)₁₀, respectively, also led to both a reduction in ribosome binding and 100S formation (Fig EV4C–E), suggesting that the sequence and not just the length of the linker is critical for BsHHPF activity. Lastly, we also monitored 100S formation in the *Bs*168 strain expressing the BsHHPF-F160E variant. As expected, no increase in the 100S peak or decrease in the polysome peaks was observed upon BsHHPF-F160E induction (Fig 5G), indicating that BsHHPF-CTD homodimerization is necessary for 100S formation.

Further support for the loss of activity of the BsHHPF-L Δ 20AA and BsHHPF-F160E variants comes from growth assays. Compared to the wild-type *Bs*168 strain, the Δ BsHHPF strain exhibits a lag phase when stationary phase cells are diluted into fresh media (Fig 5H), as reported previously (Akanuma *et al.*, 2016). The lag phenotype can be restored by expression of wild-type BsHHPF, but not by BsHHPF-L Δ 20AA and BsHHPF-F160E variants (Fig 5H). Curiously, the BsHHPF-L Δ 10AA variant also rescued the growth phenotype (Fig 5H), suggesting that ribosome binding rather than

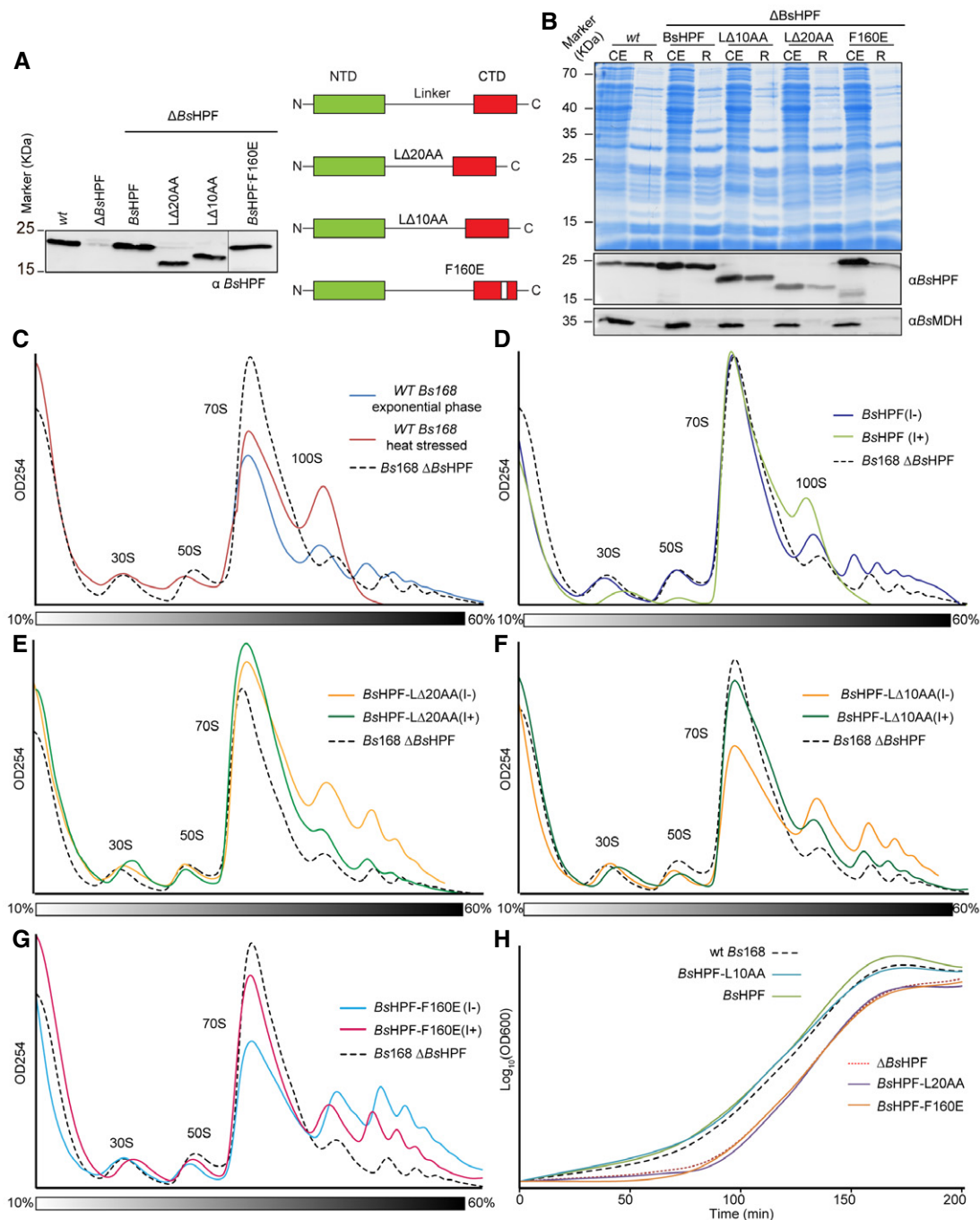


Figure 5. Monitoring 100S formation *in vivo* for BsHPF variants.

- A Western blot using antibodies raised against BsHPF to assess the levels of BsHPF in cell extracts of wild-type *Bs168* (wt), Δ BsHPF, and Δ BsHPF strains expressing either wild-type BsHPF or BsHPF- Δ 20AA, BsHPF- Δ 10AA, BsHPF-F160E variants.
- B Coomassie (above) and Western blot of cell extracts (CE) and ribosome pelleted fractions (R) of the wild-type *Bs168* (wt) strain or the Δ BsHPF strains expressing either wild-type BsHPF, BsHPF- Δ 10AA, BsHPF- Δ 20AA, and BsHPF-F160E.
- C Sucrose gradient profiles of cell extracts from the wild-type *Bs168* (wt) strain in exponential phase (blue) or heat stressed (red), compared with the extract from the *Bs168* Δ BsHPF strain (dashed line).
- D–G Sucrose gradient profiles of cell extracts from the (D) *Bs168* Δ BsHPF amyE::BsHPF strain, (E) *Bs168* Δ BsHPF amyE::BsHPF- Δ 20AA strain, (F) *Bs168* Δ BsHPF amyE::BsHPF- Δ 10AA strain, and (G) *Bs168* Δ BsHPF amyE::BsHPF-F160E strain in the absence (–) or presence (+) of IPTG. The dashed line of the *Bs168* Δ BsHPF strain from (C) is shown for reference.
- H Growth curves illustrating the recovery from stationary phase of the wild-type *Bs168* (wt), Δ BsHPF, and Δ BsHPF strains expressing either wild-type BsHPF or BsHPF- Δ 20AA, BsHPF- Δ 10AA, BsHPF-F160E variants.

Source data are available online for this figure.

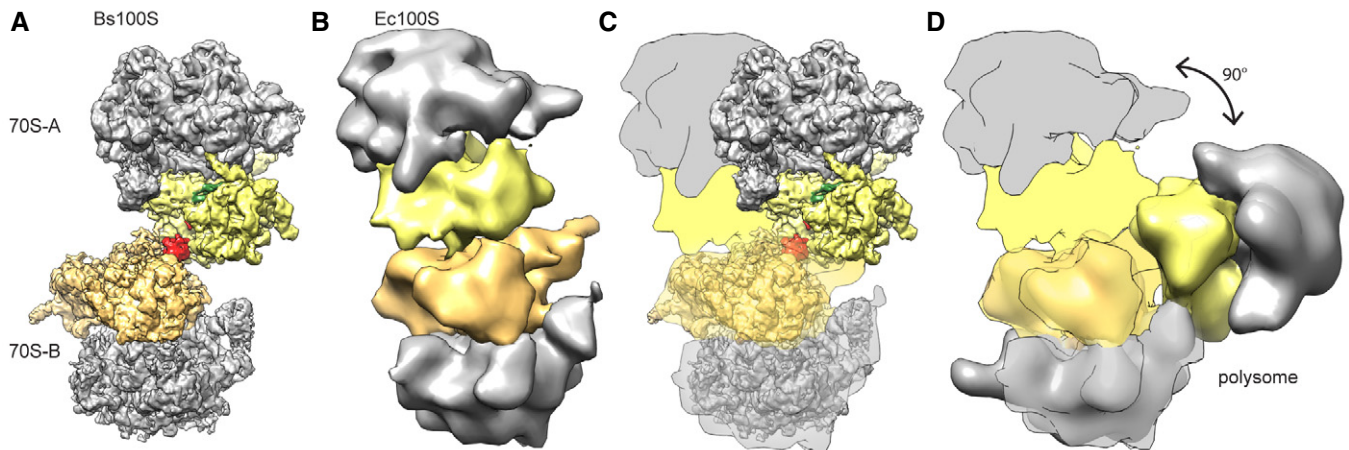


Figure 6. Spatial organization of Bs100S, Ec100S, and polysomes.

A–D Comparison of the 70S-A and 70S-B monomer arrangement in (A) Bs100S, compared with (B, C) Ec100S (Ortiz *et al*, 2010) and (D) *Escherichia coli* polysomes (Brandt *et al*, 2009). The 30S-A (yellow), 30S-B (orange), 50S (gray), BsHHPF-NTD (green), and BsHHPF-CTD (red) are colored for reference, and schematics of the Ec100S are presented in (C) and (D) for ease of comparison.

100S formation may be important for efficient stationary phase recovery.

Distinct arrangement of 70S monomers in the Bs100S

In order to obtain a reconstruction of the complete Bs100S particle to compare with previous Ec100S reconstructions, we also reprocessed the cryo-EM data using a larger box size that completely encompassed both 70S monomers (Fig EV2). Despite the inherent flexibility between the 70S monomers, we were able to obtain a reconstruction of the Bs100S (Fig 6A) with an average resolution of 6.2 Å (Fig EV5A–C). The relative orientation of the 70S-A and 70S-B monomers within the Bs100S was related by a 180° rotational symmetry with the axis of rotation centered on the dimeric BsHHPF-CTD (Fig EV5D). As expected, we observed additional density for the HHPF-NTD within the intersubunit space and for the HHPF-CTD at the back of the 30S subunit (Fig EV5E and F). Comparison of the Bs100S with the previous cryo-EM and cryo-ET reconstructions of the Ec100S (Fig 6B) revealed a dramatically different monomer arrangement (Fig 6C). While Ec100S dimerization involves a “back-to-back” interaction of the 30S subunits of each 70S monomers, Bs100S dimerization involves a more “side-to-side” (platform-to-platform) interaction of the 30S subunits. In the Ec100S, dimerization is proposed to be stabilized by contacts between S2 on one 70S with the cavity formed by S3/S4/S5 on the other (Kato *et al*, 2010), which may be facilitated by a swivel movement of the head of the 30S subunit that was observed upon RMF binding (Polikanov *et al*, 2012). In contrast, the head position of the Bs100S is identical to that observed in the classic post-translocational state ribosome (Sohmen *et al*, 2015) and, unlike RMF, the BsHHPF-CTD directly comprises part of the dimerization interface. The spatial orientation of the 70S monomers in the Bs100S (Fig 6A) could be considered intermediate between that observed in the Ec100S (Fig 6B; Kato *et al*, 2010) and the orientation observed in the cryo-ET reconstructions of *E. coli* polysomes (Fig 6D; Brandt *et al*, 2009).

Discussion

The appearance of hibernating 100S ribosomes is a near universal response of bacteria to adapt to a variety of stress conditions, in particular nutrient limitation (Ueta *et al*, 2013; Yoshida & Wada, 2014). Under these circumstances, bacteria employ second messenger signaling molecules, such as (p)ppGpp and cyclic AMP (cAMP), to reprogram the cellular activity network, down-regulating genes associated with translation and up-regulating stress response and amino acid biogenesis pathways (Haurlyuk *et al*, 2015; Steinchen & Bange, 2016). In *E. coli*, transcription of *rmf*, the gene encoding RMF, is up-regulated by (p)ppGpp when amino acids become limiting (Izutsu *et al*, 2001) and by cAMP upon carbon starvation (Shimada *et al*, 2013). Transcription of *yvyD*, the gene encoding BsLHPF, is under the control of the sigma factors σ^H and σ^B (Drzewiecki *et al*, 1998; Tam le *et al*, 2006; Akanuma *et al*, 2016), and up-regulated by the presence of the alarmone (p)ppGpp (Eymann *et al*, 2001; Tagami *et al*, 2012; Shimada *et al*, 2013; Fig 7A). Similarly, in the cyanobacterium *Synechococcus elongatus*, LHPF is also up-regulated by (p)ppGpp to enable dark adaptation (Hood *et al*, 2016).

The up-regulation of LHPF leads to increased 100S formation, indicating that LHPF competes effectively with translation factors, as evidenced by LHPF inhibition of *in vitro* translation systems (Ueta *et al*, 2013; Basu & Yap, 2016). Since we observed that BsHHPF is dimeric in solution, we favor a model whereby dimeric BsHHPF interacts independently with two 70S ribosomes (Fig 7B). In this model, we propose that BsHHPF utilizes the free NTDs and long linker to initially bring 70S ribosomes into close proximity, and then further stabilizes the 70S dimer using the BsHHPF-CTD ribosome interface (Fig 7B). However, we cannot exclude that at a fraction of BsHHPF resides as a monomer *in vivo*, and these BsHHPF monomers bind separately to the 70S ribosome, such that 100S formation could then occur concomitantly with BsHHPF-CTD homodimerization. Moreover, it remains unclear how hibernating 100S ribosomes exactly provide protection against stress. What is

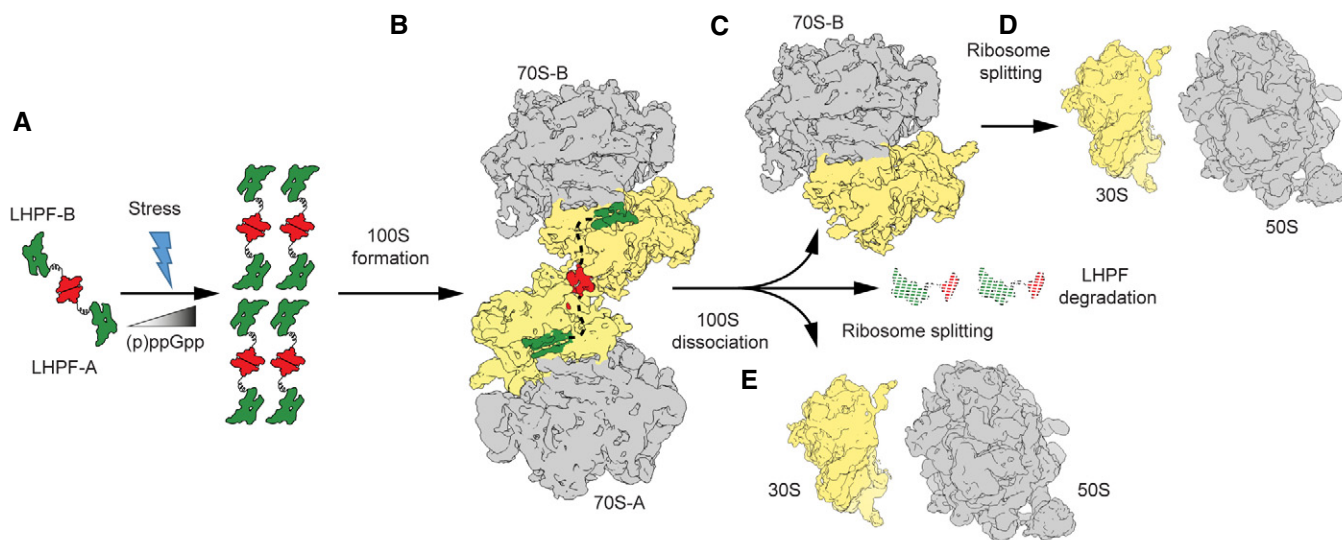


Figure 7. Model for BsHPF-induced 100S formation.

- A** Stress conditions, such as nutrient deprivation, lead to elevated levels of (p)ppGpp, which up-regulates expression of the LHPF (NTD, green; CTD, red). The LHPF-CTD can interact to form homodimers in solution and therefore may also be present as dimers in the cell.
- B** The long linker of the dimeric LHPF enables the LHPF-NTD to interact with two independent 70S ribosomes and by bringing them in to close proximity stabilizes the 70S dimers, forming 100S.
- C–E** Following removal of the stress conditions, BsHPF levels decline leading to (C) dissociation of 100S into 70S ribosomes and (D) eventually ribosome splitting into 30S and 50S subunits, or (E) alternatively directly in 30S and 50S subunits.

clear however is that in the absence of 100S, 70S ribosomes are slowly degraded leading to early cell death, suggesting that hibernating 100S are less susceptible to degradation by RNases (Fukuchi *et al*, 1995; Wada, 1998; Niven, 2004; Shcherbakova *et al*, 2015; Akanuma *et al*, 2016). Because 100S formation does not significantly alter the large rRNA surface exposed to RNases, we believe LHPF binding and 100S formation may interfere with a specific ribosome degradation pathway, rather than preventing non-specific RNase action on ribosomes. The identification of BsHPF variant, such as the BsHPF- Δ L10AA, which binds to the ribosome but does not promote 100S formation, may allow the contribution of these activities to ribosome protection to be dissected further.

In *E. coli*, disassembly of 100S is rapid and occurs within 1 min upon transfer to fresh medium, suggesting that an active mechanism exists to remove EchPF and Rmf from the ribosome (Wada, 1998; Aiso *et al*, 2005). In contrast, Bs100S are more stable than Ec100S (Ueta *et al*, 2013) and upon transfer to fresh media significant dissociation of Bs100S was only observed after 120 min, where LHPF protein levels were also significantly decreased (Akanuma *et al*, 2016). Nevertheless, recycling factors, such as IF3, RRF, and EF-G, which have been reported to remove LHPF (PSRP-1) from Spinach chloroplast ribosomes (Sharma *et al*, 2010), might also be involved in BsHPF release and 100S dissociation (Fig 7C–E).

In conclusion, the high conservation of the LHPF proteins suggests that most, if not all, LHPF proteins are present as dimers in the cell, with the implication that the majority of bacteria are likely to utilize an identical mechanism to induce 100S formation as we have described here for *B. subtilis* (Fig 7).

Materials and Methods

Cloning of BsHPF and BsHPF variants for protein purification

The *yyvD* gene encoding BsHPF was amplified from *B. subtilis* PY79 genomic DNA by polymerase chain reaction using Phusion High-Fidelity DNA Polymerase (NEB) according to the manufacturer's manual. The *forward* primer encoded a hexa-histidine tag in-frame with the DNA sequence of *yyvD*. The fragment was cloned via *NcoI/XhoI* restriction sites into a modified pGAT2-vector incorporating a GST-tag N-terminal of His₆-BsHPF. BsHPF-CTD (amino acids 130–189 of BsHPF), BsHPF-NTD (amino acids 1–104 of BsHPF), and BsHPF(F160E) containing an N-terminal hexa-histidine tag were amplified by PCR as described above and cloned via *NcoI/XhoI* restriction sites into pET24d(+) vector (Novagen). Mutations within BsHPF were introduced by overlapping PCR.

Protein production and purification for SEC and SLS

Escherichia coli BL21(DE3) cells (NEB) carrying the expression plasmid were grown in lysogeny broth (LB) medium supplemented with ampicillin (100 μ g/ml) or kanamycin (50 μ g/ml) and D(+)-lactose-monohydrate (12.5 g/l) for 16 h at 30°C under rigorous shaking (180 rpm). The cells were harvested (3,500 \times g, 20 min, 4°C), resuspended in lysis buffer (20 mM HEPES-KOH, pH 8.0, 20 mM KCl, 20 mM MgCl₂, 500 mM NaCl, 40 mM imidazole) and lysed using a M-110L Microfluidizer (Microfluidics). After centrifugation (47,850 \times g, 20 min, 4°C), the clear supernatant was loaded on a HisTrap HP 1 ml column (GE Healthcare) equilibrated with 15 column volumes (CV) of lysis buffer. After

washing with 15 CV of lysis buffer, the protein was eluted with 5 CV of elution buffer (lysis buffer containing 500 mM imidazole). The GST-tag was removed from BsHPF variants by incubation with 100 U of bovine thrombin (Merck Millipore) for 2 h at 20°C. After dilution with 12 volume parts of lysis buffer without imidazole, BsHPF variants were resubjected to Ni-NTA affinity chromatography as described above and the elution fraction containing BsHPF were collected. BsHPF and BsHPF variants were then concentrated using an Amicon Ultracel-10K or 3K, respectively (Merck Millipore), and applied to size-exclusion chromatography (HiLoad 26/600 Superdex 75 pg, GE Healthcare) equilibrated in SEC buffer (20 mM HEPES-KOH, pH 8.0, 20 mM KCl, 20 mM MgCl₂, 500 mM NH₄Cl). Protein-containing fractions were pooled and concentrated to ~500 μM as determined by a spectrophotometer (NanoDrop Lite, Thermo Scientific).

Analysis of oligomerization states of BsHPF variants by SEC and SLS

The apparent molecular weight was analyzed by size-exclusion chromatography using a HiLoad 26/600 Superdex 75 pg column (GE Healthcare) equilibrated in SEC buffer. A standard curve for molecular mass determination was obtained using BSA (66.5 kDa), ovalbumin (chicken, 44.3 kDa), myoglobin (horse, 17 kDa), and vitamin B12 (1.35 kDa). The absolute molecular weight was determined by static light scattering (SLS) with a DelsaMax CORE (Beckmann Coulter) according to the manufacturer's instructions.

Cloning of BsHPF and BsHPF variants for *in vivo* studies

Full-length *yvyD* was amplified from genomic DNA by PCR as described above with the forward primer encoding the strong ribosomal binding site of the *gstB* gene (AGGAGGAATCAAAA) and cloned via *Sall*/*SphI* restriction sites into the pDR111 plasmid (Ben-Yehuda et al, 2003). The BsHPF-LΔ10AA, BsHPF-LΔ20AA, and BsHPF-F160E mutation were introduced by overlap extension PCR and cloned via *Sall*/*SphI* restriction sites as described above. The resulting plasmids were linearized by digestion with *ScaI* and transformed into naturally competent *B. subtilis* cells. Proper integration into the *amyE* locus was checked by growing selected transformants on LB-Agar containing 1% starch overnight and staining the plates with a solution of 0.5% (w/v) iodine, 1% (w/v) potassium iodine. Strains and oligonucleotides used in this study are presented in Tables EV2 and EV3.

Western blotting of BsHPF variants

Strains expressing HPF variants *in trans* were grown in LB medium supplemented with 1 mM IPTG with rigorous shaking to until the mid-exponential phase (OD₆₀₀ of ~0.8), harvested by centrifugation at 11,000 × g, 4°C for 5 min, washed once in TE buffer (10 mM Tris-HCl, 1 mM EDTA, pH 8.0), and disrupted by sonication three times for 30 s on ice in TE buffer supplemented with 1 mM PMSF. The soluble protein was cleared from cell debris by centrifugation at 11,000 × g, 4°C for 5 min. 10 μg of the protein extract (as determined by the Bradford assay) was analyzed by SDS-PAGE and Western Blotting onto a nitrocellulose membrane. As controls, equally treated samples from a stationary

phase overnight culture of *B. subtilis* wild-type or *Δhpf* cells were loaded. The BsHPF protein was detected using a polyclonal antibody raised against BsHPF (Pineda Antibody Service) and a polyclonal Goat anti-Rabbit IgG alkaline Phosphatase conjugated antibody (Antikörper Online). Western blotting using an antibody against the malate dehydrogenase (MDH) was used as a loading control. The ECF reagent (GE Healthcare) was used as a substrate according to the manufacturer's manual, and chemifluorescent signals were detected using a cooled CCD camera in a ChemiBIS 4.2 Bioimaging system (DNR).

Binding assay for BsHPF variants with pelleted ribosomes

Bacillus subtilis cells were grown in 200-ml LB medium supplemented with 1 mM IPTG with rigorous shaking (200 rpm) to the mid-exponential phase (OD₆₀₀ ~0.8) and harvested by centrifugation at 15,300 × g, 10 min, 4°C. Ribosomes were pelleted as described in (Schmalisch et al, 2002). Briefly, cells were washed once in buffer A (20 mM Tris-HCl, 100 mM NH₄Cl, 10 mM MgCl₂, 10 mM 2-mercaptoethanol, pH 7.5), resuspended in 3 ml of the same buffer with 1 mM PMSF and disrupted in a French Pressure Cell three times at 1,000 psi. The lysate was cleared from cell debris by centrifugation for 30 min at 29,953 × g, 4°C (SW55-Ti, Beckman Coulter), layered on top of a 8 ml 1.1 M sucrose cushion in buffer A, and centrifuged for 16 h at 119,307 × g, 4°C (SW40-Ti, Beckman Coulter). The cell pellet was washed three times in buffer A and resuspended in buffer B (20 mM Tris-HCl, 100 mM NH₄Cl, 6 mM MgCl₂, 2 mM DTT). The suspension was centrifuged at 10,000 × g, 10 min, 4°C, and the supernatant containing the ribosomes was collected. 10 μg of the total soluble protein ("CE", as determined by the Bradford assay) and an equal volume of the ribosome suspension ("R") was subjected to 15% SDS-PAGE and subsequent stained with Coomassie using standard procedures or Western blotting as described above.

Growth recovery from stationary phase

Precultures of *B. subtilis* cells were grown in 5-ml LB medium supplemented with 0.5 mM IPTG at 37°C for 18 h, to ensure the cells reached the stationary growth phase. The cultures were then diluted to an OD₆₀₀ of 0.05 into 20-ml fresh LB medium and grown at 37°C with rigorous shaking. The cell growth was monitored by determining the optical density at 600 nm (OD₆₀₀) at regular intervals.

Sucrose density gradient centrifugation analysis

Analysis of 100S formation was performed as described previously for *B. subtilis* (Akanuma et al, 2016). Briefly, 50-ml LB medium was inoculated at a 1:100 dilution with an overnight culture. Expression was induced using 1 mM IPTG at an OD₆₀₀ of 0.4. Cells were harvested at the stationary phase by centrifugation at 4,000 × g for 10 min at 4°C (Hettich Rotanta 46R) and the cell pellet re-suspended in buffer C (50 mM HEPES-KOH, pH7.4, 100 mM KOAc, 25 mM Mg (OAc)₂, 6 mM β-mercaptoethanol). Cells were lysed using the sonifier three times, with each cycle consisting of 30 s at 30% power followed by centrifugation at 16,000 × g for 15 min at 4°C to remove cellular debris. A total OD₂₆₀ of 10 of the cleared lysate was loaded onto sucrose density gradients (10–60% sucrose in buffer C)

by centrifugation at $154,693 \times g$ (SW-40 Ti, Beckman Coulter) for 3 h at 4°C and then analyzed using a Gradient Station (Bio-comp) with an Econo UV Monitor (Bio-Rad) and a FC203B Fraction Collector (Gilson).

Preparation of *Bacillus subtilis* S12 extract

Bacillus subtilis S12 extract was prepared as described (Sohmen *et al.*, 2015). Briefly, an “INFORCE HT minifors” bench top fermenter was used to grow *B. subtilis* strain 168 cells to an OD_{600} 4.5 in $2 \times$ YPTG medium (16 g/l peptone, 10 g/l yeast extract, 5 g/l NaCl, 22 mM NaH_2PO_4 , 40 mM Na_2HPO_4 , 19.8 g/l glucose (sterile filtered)), with extra glucose feeding at 37°C while maintaining a pH 7.0 and oxygen level (60%). After collecting cells at $5,000 \times g$ at 4°C for 15 min, they were washed $3 \times$ in cold Buffer A (10 mM Tris-acetate (pH 8.2), 14 mM magnesium acetate, 60 mM potassium glutamate, 1 mM dithiothreitol, and 6 mM β -mercaptoethanol). Cells were then snap-frozen in liquid nitrogen and stored at $-80^\circ C$. 15 g of cells was thawed on ice, resuspended in 10 ml of cold buffer B (buffer A missing β -mercaptoethanol), and lysed $3 \times$ at 15,000 psi in a “microfluidics model 110I lab homogenizer”. The lysate was cleared at $12,000 \times g$ and 4°C for 10 min and incubated in a water bath for 30 min at 37°C. The cell extract was aliquoted, snap-frozen, and stored at $-80^\circ C$. Extracts were analyzed on sucrose density gradients (10–50% sucrose in buffer C), by centrifugation at $89,454 \times g$ (SW-28, Beckman Coulter) for 4 h at 4°C. For 100S purification, 100S fractions were collected using a Gradient Station (Bio-comp) with an Econo UV Monitor (Bio-Rad) and a FC203B Fraction Collector (Gilson). Purified 100S ribosomes were concentrated by centrifugation at $92,159 \times g$ for 2.5 h at 4°C (TLA110 rotor, Beckman Coulter).

Negative stain electron microscopy

Ribosomal particles were diluted in buffer C to a final concentration of 0.2 OD_{260}/ml . A 3.5 μl sample was applied onto a carbon-coated grid. After 30 s, the grids were washed with distilled water and then stained with 2% aqueous uranyl acetate for 15 s. The remaining liquid was removed by touching the grid with filter paper. Micrographs were taken using a Morgagni transmission electron microscope (FEI).

Cryo-electron microscopy and single particle reconstruction

A total of 4 OD_{260}/ml *Bs100S* sample were applied to 2 nm pre-coated Quantifoil R3/3 holey carbon-supported grids and vitrified using Vitrobot Mark IV (FEI Company). Data collection was performed using EM-TOOLS (TVIPS GmbH) on a Titan Krios transmission electron microscope equipped with a Falcon II direct electron detector (FEI Company) at 300 kV at a pixel size of 1.084 Å and a defocus range of 0.7–2.2 μm . Ten frames (dose per frame of 2.5 $e^-/\text{Å}$) were aligned using Motion Correction Software (Li *et al.*, 2013). Power-spectra, defocus values, and astigmatism were then determined using CTFFIND4 software (Rohou & Grigorieff, 2015). Micrographs showing Thon rings beyond 3.5 Å were manually inspected for a good areas and power-spectra quality. Automatic particle picking was then performed using SIGNATURE (Chen & Grigorieff, 2007), and single particles were windowed out in small

box able to contain a 70S ribosome together with the majority of the small 30S subunit of the neighboring 70S ribosome. The particles were then further processed using FREALIGN (Grigorieff, 2007). The 253,905 particles were first subjected to an extensive 3D classification (Fig EV2A and B), and the selected 24,546 *Bs100S* particles of class 8 were then subjected to refinement using 30S-70S mask resulting in a final reconstruction of 3.8 Å (0.143 FSC) average resolution (Figs EV2C and EV3). Local resolution was finally calculated using ResMap (Kucukelbir *et al.*, 2014). For the processing of the complete *Bs100S*, the coordinates of the selected 24,546 particles were carefully re-inspected in order to remove particles that were within close proximity of another particle, so as not to include particles twice in the final reconstruction; 5,511 particles were identified and removed from class 8, and the rest of particles were windowed out using a larger box size that encompassed two 70S ribosomes (Fig EV2D). The remaining 19,335 particles were then realigned and refined, resulting in a final reconstruction with an average resolution of 6.2 Å (0.143 FSC; Fig EV5A–C).

Molecular modeling, refinement, and validation

The molecular model for the ribosomal proteins and rRNA of the 70S ribosome of the *Bs100S* was based on the molecular model from the recent cryo-EM reconstruction of the *B. subtilis* 70S ribosome (PDB ID 3JW9; Sohmen *et al.*, 2015). The molecular model was fitted as a rigid body into the cryo-EM density maps using UCSF Chimera (Pettersen *et al.*, 2004). For *BsHPPF*-NTD domain, a homology model was generated using HHPred (Soding *et al.*, 2005) based on the HPP protein template from *E. coli* (PDB ID 4V8H; Polikanov *et al.*, 2012; Fig EV1C). Molecular models were fitted and adjusted by using COOT (Emsley & Cowtan, 2004) and refined in Phenix using *phenix.real_space_refine* (Adams *et al.*, 2010). Model over-fitting was evaluated through its refinement against one cryo-EM half map as described previously (Brown *et al.*, 2015). FSC curves were calculated between the resulting model and the half map used for refinement, as well as between the resulting model and the other half map for cross-validation (Fig EV3E). The final refinement statistics were determined using MolProbity (Chen *et al.*, 2010) and are provided in Table EV1. For *BsHPPF*-CTD domain, a homology model was generated using HHPred based on the template from *C. acetobutylicum* (PDB ID 3KA5; Fig EV1D). The molecular model was rigid body fitted using UCSF Chimera (Pettersen *et al.*, 2004).

Figure preparation

Figures showing map densities and atomic models were generated using UCSF Chimera (Pettersen *et al.*, 2004).

Accession numbers

The cryo-EM map of the *Bs70S*-30S subcomplex and the complete *Bs100S* have been deposited in the EMDB with the accession codes EMD-3656 and EMD-3664, respectively. Atomic coordinates have been deposited in the Protein Data Bank with accession code PDB ID 5NJT.

Expanded View for this article is available online.

Acknowledgements

We thank Heidimarie Sieber, Charlotte Ungewickell, and Susanne Rieder for expert technical assistance; Uwe Linne (Marburg) for mass spectrometry support; and Beckmann-Coulter GmbH (Krefeld, Germany) for kindly providing the DelsaMax CORE. This research was supported by grants from the Deutsche Forschungsgemeinschaft (SPP-1879 to K.T., G.B., and D.N.W.).

Author contributions

DNW, GB, and KT designed and supervised the study. MA prepared the Bs100S sample for cryo-EM and performed all sucrose gradient analyses. OB collected the cryo-EM data. BB, MA, and SA processed the cryo-EM data. BB, MA, RB, and DNW interpreted the cryo-EM data. WS cloned and purified the BsHPF protein variants and performed the SEC and SLS. HS generated all BsHPF expression strains and performed Western blotting, growth curves, and ribosome pelleting assays. DNW, GB, and KT wrote the manuscript with comments from all authors.

Conflict of interest

The authors declare that they have no conflict of interest.

Note added in proof

The recent cryo-EM structure of the *Staphylococcus aureus* 100S determined by Khusainov et al (2017) reveals that the mechanism of 70S dimerization mediated by the *S. aureus* long-form HPF appears to be similar to that observed here for *Bacillus subtilis*.

References

- Adams PD, Afonine PV, Bunkoczi G, Chen VB, Davis IW, Echols N, Headd JJ, Hung LW, Kapral GJ, Grosse-Kunstleve RW, McCoy AJ, Moriarty NW, Oeffner R, Read RJ, Richardson DC, Richardson JS, Terwilliger TC, Zwart PH (2010) PHENIX: a comprehensive python-based system for macromolecular structure solution. *Acta Crystallogr D Biol Crystallogr* 66(Pt 2): 213–221
- Agafonov DE, Spirin AS (2004) The ribosome-associated inhibitor A reduces translation errors. *Biochem Biophys Res Commun* 320: 354–358
- Aiso T, Yoshida H, Wada A, Ohki R (2005) Modulation of mRNA stability participates in stationary-phase-specific expression of ribosome modulation factor. *J Bacteriol* 187: 1951–1958
- Akanuma G, Kazo Y, Tagami K, Hiraoka H, Yano K, Suzuki S, Hanai R, Nanamiya H, Kato-Yamada Y, Kawamura F (2016) Ribosome dimerization is essential for the efficient regrowth of *Bacillus subtilis*. *Microbiology* 162: 448–458
- Basu A, Yap MN (2016) Ribosome hibernation factor promotes Staphylococcal survival and differentially represses translation. *Nucleic Acids Res* 44: 4881–4893
- Ben-Yehuda S, Rudner DZ, Losick R (2003) RacA, a bacterial protein that anchors chromosomes to the cell poles. *Science* 299: 532–536
- Bieri P, Leibundgut M, Saurer M, Boehringer D, Ban N (2017) The complete structure of the chloroplast 70S ribosome in complex with translation factor pY. *EMBO J* 36: 475–486
- Brandt F, Etchells SA, Ortiz JO, Elcock AH, Hartl FU, Baumeister W (2009) The native 3D organization of bacterial polysomes. *Cell* 136: 261–271
- Brown A, Long F, Nicholls RA, Toots J, Emsley P, Murshudov G (2015) Tools for macromolecular model building and refinement into electron cryo-microscopy reconstructions. *Acta Crystallogr D Biol Crystallogr* 71(Pt 1): 136–153
- Chen JZ, Grigorieff N (2007) SIGNATURE: a single-particle selection system for molecular electron microscopy. *J Struct Biol* 157: 168–173
- Chen VB, Arendall WB III, Headd JJ, Keedy DA, Immormino RM, Kapral GJ, Murray LW, Richardson JS, Richardson DC (2010) MolProbity: all-atom structure validation for macromolecular crystallography. *Acta Crystallogr D Biol Crystallogr* 66(Pt 1): 12–21
- Drzewiecki K, Eymann C, Mittenhuber G, Hecker M (1998) The *yyvD* gene of *Bacillus subtilis* is under dual control of sigmaB and sigmaH. *J Bacteriol* 180: 6674–6680
- El-Sharoud WM, Niven GW (2007) The influence of ribosome modulation factor on the survival of stationary-phase *Escherichia coli* during acid stress. *Microbiology* 153(Pt 1): 247–253
- Emsley P, Cowtan K (2004) Coot: model-building tools for molecular graphics. *Acta Crystallogr D Biol Crystallogr* 60: 2126–2132
- Eymann C, Mittenhuber G, Hecker M (2001) The stringent response, sigmaH-dependent gene expression and sporulation in *Bacillus subtilis*. *Mol Gen Genet* 264: 913–923
- Fukuchi JI, Kashiwagi K, Yamagishi M, Ishihama A, Igarashi K (1995) Decrease in cell viability due to the accumulation of spermidine in spermidine acetyltransferase-deficient mutant of *Escherichia coli*. *J Biol Chem* 270: 18831–18835
- Garay-Arroyo A, Colmenero-Flores JM, Garciarrubio A, Covarrubias AA (2000) Highly hydrophilic proteins in prokaryotes and eukaryotes are common during conditions of water deficit. *J Biol Chem* 275: 5668–5674
- Graf M, Arenz S, Huter P, Donhofer A, Novacek J, Wilson DN (2016) Cryo-EM structure of the spinach chloroplast ribosome reveals the location of plastid-specific ribosomal proteins and extensions. *Nucleic Acids Res* 45: 2887–2896
- Grigorieff N (2007) FREALIGN: high-resolution refinement of single particle structures. *J Struct Biol* 157: 117–125
- Haurlyuk V, Atkinson GC, Murakami KS, Tenson T, Gerdes K (2015) Recent functional insights into the role of (p)ppGpp in bacterial physiology. *Nat Rev Microbiol* 13: 298–309
- Hood RD, Higgins SA, Flamholz A, Nichols RJ, Savage DF (2016) The stringent response regulates adaptation to darkness in the cyanobacterium *Synechococcus elongatus*. *Proc Natl Acad Sci USA* 113: E4867–E4876
- Izutsu K, Wada A, Wada C (2001) Expression of ribosome modulation factor (RMF) in *Escherichia coli* requires ppGpp. *Genes Cells* 6: 665–676
- Jenner L, Demeshkina N, Yusupova G, Yusupov M (2011) Structural rearrangements of the ribosome at the tRNA proofreading step. *Nat Struct Mol Biol* 17: 1072–1078
- Kato T, Yoshida H, Miyata T, Maki Y, Wada A, Namba K (2010) Structure of the 100S ribosome in the hibernation stage revealed by electron cryomicroscopy. *Structure* 18: 719–724
- Khusainov I, Vicens Q, Ayupov R, Usachev K, Myasnikov A, Simonetti A, Validov S, Kieffer B, Yusupova G, Yusupov M, Hashem Y (2017) Structures and dynamics of hibernating ribosomes from *Staphylococcus aureus* mediated by intermolecular interactions of HPF. *EMBO J* 36: 2073–2087
- Kline BC, McKay SL, Tang WW, Portnoy DA (2015) The listeria monocytogenes hibernation-promoting factor is required for the formation of 100S ribosomes, optimal fitness, and pathogenesis. *J Bacteriol* 197: 581–591
- Kucukelbir A, Sigworth FJ, Tagare HD (2014) Quantifying the local resolution of cryo-EM density maps. *Nat Methods* 11: 63–65
- Li X, Mooney P, Zheng S, Booth CR, Braumfeld MB, Gubbens S, Agard DA, Cheng Y (2013) Electron counting and beam-induced motion correction

- enable near-atomic-resolution single-particle cryo-EM. *Nat Methods* 10: 584–590
- Maki Y, Yoshida H, Wada A (2000) Two proteins, YfiA and YhbH, associated with resting ribosomes in stationary phase *Escherichia coli*. *Genes Cells* 5: 965–974
- McKay SL, Portnoy DA (2015) Ribosome hibernation facilitates tolerance of stationary-phase bacteria to aminoglycosides. *Antimicrob Agents Chemother* 59: 6992–6999
- Niven GW (2004) Ribosome modulation factor protects *Escherichia coli* during heat stress, but this may not be dependent on ribosome dimerization. *Arch Microbiol* 182: 60–66
- Ortiz JO, Brandt F, Matias VR, Sennels L, Rappsilber J, Scheres SH, Eibauer M, Hartl FU, Baumeister W (2010) Structure of hibernating ribosomes studied by cryoelectron tomography *in vitro* and *in situ*. *J Cell Biol* 190: 613–621
- Pei J, Kim BH, Grishin NV (2008) PROMALS3D: a tool for multiple protein sequence and structure alignments. *Nucleic Acids Res* 36: 2295–2300
- Pettersen EF, Goddard TD, Huang CC, Couch GS, Greenblatt DM, Meng EC, Ferrin TE (2004) UCSF chimera – a visualization system for exploratory research and analysis. *J Comput Chem* 25: 1605–1612
- Polikanov YS, Blaha GM, Steitz TA (2012) How hibernation factors RMF, HPF, and YfiA turn off protein synthesis. *Science* 336: 915–918
- Puri P, Eckhardt TH, Franken LE, Fusetti F, Stuart MC, Boekema EJ, Kuipers OP, Kok J, Poolman B (2014) *Lactococcus lactis* YfiA is necessary and sufficient for ribosome dimerization. *Mol Microbiol* 91: 394–407
- Reiss S, Pane-Farre J, Fuchs S, Francois P, Liebecke M, Schrenzel J, Lindequist U, Lalk M, Wolz C, Hecker M, Engelmann S (2012) Global analysis of the *Staphylococcus aureus* response to mupirocin. *Antimicrob Agents Chemother* 56: 787–804
- Rohou A, Grigorieff N (2015) CTFIND4: fast and accurate defocus estimation from electron micrographs. *J Struct Biol* 192: 216–221
- Schmalisch M, Langbein I, Stulke J (2002) The general stress protein Ctc of *Bacillus subtilis* is a ribosomal protein. *J Mol Microbiol Biotechnol* 4: 495–501
- Sharma MR, Wilson DN, Datta PP, Barat C, Schluenzen F, Fucini P, Agrawal RK (2007) Cryo-EM study of the spinach chloroplast ribosome reveals the structural and functional roles of plastid-specific ribosomal proteins. *Proc Natl Acad Sci USA* 104: 19315–19320
- Sharma MR, Donhofer A, Barat C, Marquez V, Datta PP, Fucini P, Wilson DN, Agrawal RK (2010) PSRP1 is not a ribosomal protein, but a ribosome-binding factor that is recycled by the ribosome-recycling factor (RRF) and elongation factor G (EF-G). *J Biol Chem* 285: 4006–4014
- Shcherbakova K, Nakayama H, Shimamoto N (2015) Role of 100S ribosomes in bacterial decay period. *Genes Cells* 20: 789–801
- Shimada T, Yoshida H, Ishihama A (2013) Involvement of cyclic AMP receptor protein in regulation of the *rmf* gene encoding the ribosome modulation factor in *Escherichia coli*. *J Bacteriol* 195: 2212–2219
- Soding J, Biegert A, Lupas AN (2005) The HHpred interactive server for protein homology detection and structure prediction. *Nucleic Acids Res* 33(Web Server issue): W244–W248
- Sohmen D, Chiba S, Shimokawa-Chiba N, Innis CA, Berninghausen O, Beckmann R, Ito K, Wilson DN (2015) Structure of the *Bacillus subtilis* 70S ribosome reveals the basis for species-specific stalling. *Nat Commun* 6: 6941
- Steinchen W, Bange G (2016) The magic dance of the alarmones (p)ppGpp. *Mol Microbiol* 101: 531–544
- Tagami K, Nanamiya H, Kazo Y, Maehashi M, Suzuki S, Namba E, Hoshiya M, Hanai R, Tozawa Y, Morimoto T, Ogasawara N, Kageyama Y, Ara K, Ozaki K, Yoshida M, Kuroiwa H, Kuroiwa T, Ohashi Y, Kawamura F (2012) Expression of a small (p)ppGpp synthetase, YwaC, in the (p)ppGpp(0) mutant of *Bacillus subtilis* triggers YvyD-dependent dimerization of ribosome. *Microbiologyopen* 1: 115–134
- Tam le T, Antelmann H, Eymann C, Albrecht D, Bernhardt J, Hecker M (2006) Proteome signatures for stress and starvation in *Bacillus subtilis* as revealed by a 2-D gel image color coding approach. *Proteomics* 6: 4565–4585
- Ueta M, Yoshida A, Wada C, Baba T, Mori H, Wada A (2005) Ribosome binding proteins YhbH and YfiA have opposite functions during 100S formation in the stationary phase of *Escherichia coli*. *Genes Cells* 10: 1103–1112
- Ueta M, Ohniwa RL, Yoshida H, Maki Y, Wada C, Wada A (2008) Role of HPF (hibernation promoting factor) in translational activity in *Escherichia coli*. *J Biochem* 143: 425–433
- Ueta M, Wada C, Wada A (2010) Formation of 100S ribosomes in *Staphylococcus aureus* by the hibernation promoting factor homolog SaHPF. *Genes Cells* 15: 43–58
- Ueta M, Wada C, Daifuku T, Sako Y, Bessho Y, Kitamura A, Ohniwa RL, Morikawa K, Yoshida H, Kato T, Miyata T, Namba K, Wada A (2013) Conservation of two distinct types of 100S ribosome in bacteria. *Genes Cells* 18: 554–574
- Vila-Sanjurjo A, Schuwirth BS, Hau CW, Cate JHD (2004) Structural basis for the control of translational initiation during stress. *Nature Struct Mol Biol* 11: 1054–1059
- Wada A, Yamazaki Y, Fujita N, Ishihama A (1990) Structure and probable genetic location of a ribosome modulation factor associated with 100S ribosomes in stationary-phase *Escherichia coli* cells. *Proc Natl Acad Sci USA* 87: 2657–2661
- Wada A, Igarashi K, Yoshimura S, Aimoto S, Ishihama A (1995) Ribosome modulation factor: stationary growth phase-specific inhibitor of ribosome functions from *Escherichia coli*. *Biochem Biophys Res Commun* 214: 410–417
- Wada A (1998) Growth phase coupled modulation of *Escherichia coli* ribosomes. *Genes Cells* 3: 203–208
- Wada A, Mikkola R, Kurland CG, Ishihama A (2000) Growth-phase coupled changes of the ribosome profile in natural isolates and laboratory strains of *Escherichia coli*. *J Bacteriol* 182: 2893–2899
- Yamagishi M, Matsushima H, Wada A, Sakagami M, Fujita N, Ishihama A (1993) Regulation of the *Escherichia coli* *rmf* gene encoding the ribosome modulation factor - growth phase-dependent and growth rate-dependent control. *EMBO J* 12: 625–630
- Yoshida H, Maki Y, Kato H, Fujisawa H, Izutsu K, Wada C, Wada A (2002) The ribosome modulation factor (RMF) binding site on the 100S ribosome of *Escherichia coli*. *J Biochem* 132: 983–989
- Yoshida H, Wada A (2014) The 100S ribosome: ribosomal hibernation induced by stress. *Wiley Interdiscip Rev RNA* 5: 723–732